 doi:10.20944/preprints202103.0464.v1

Article

Hybrid nanoparticles based on cobalt ferrite and gold: preparation and characterization

Svetlana Saikova [1,2,*], Alexander Pavlikov [1], Tatyana Trofimova [1], Yuri Mikhlin [2], Denis Karpov [1], Anastasia Asanova [3], Yuri Grigoriev [1], Mikhail Volochaev [4], Sergey Zharkov [4] and Dmitry Velikanov [4]

[1] Siberian Federal University, School of Non-Ferrous Metals and Material Science, Krasnoyarsk, 660041, Russia; apavlikov98@mail.ru (A.P.); ttv91@mail.ru (T.T.); denikarp@mail.ru (D.K.); gr2897@gmail.com (Y.G.)
[2] Institute of Chemistry and Chemical Technology, Federal Research Center "Krasnoyarsk Science Center of the Siberian Branch of the Russian Academy of Sciences", 660036 Krasnoyarsk, Russia; yumikh@icct.ru (Y.M.)
[3] Krasnoyarsk State Agrarian University, Krasnoyarsk, 660049, Russia; nastasia.asanova@gmail.com (A.A.)
[4] Kirensky Institute of Physics, Federal Research Center "Krasnoyarsk Science Center of the Siberian Branch of the Russian Academy of Sciences", Akademgorodok, 660036 Krasnoyarsk, Russia; volochaev91@mail.ru (M.V.); zharkov@iph.krasn.ru (S.Z.); dpona1@gmail.com (D.V.)
* Correspondence: ssai@mail.ru

Abstract: During the past few decades, hybrid nanoparticles (HNPs) based on a magnetic material and gold have attracted interest for applications in catalysis, diagnostics and nanomedicine. In this paper, magnetic $CoFe_2O_4$/Au HNPs with an average particle size of 10–20 nm decorated with 2-nm gold clusters were prepared using methionine as a reducer and an anchor between $CoFe_2O_4$ and gold. The obtained nanoparticles were studied by X-Ray diffraction (XRD), transmission electron microscopy (TEM), Fourier-transform infrared (FT-IR) spectroscopy and X-Ray photoelectron spectroscopy (XPS) and UV-Vis spectroscopy techniques. The TEM images of the HNPs obtained after one, six and ten gold deposition cycles showed that the surface of cobalt ferrite was covered with gold nanoclusters, which slightly increased with an increase in the number of gold deposition cycles (from 2.12 ± 0.15 nm after one cycle to 2.46 ± 0.13 nm after ten cycles) without any change in surface density. The magnetic measurements showed that the obtained HNPs possessed typical ferrimagnetic behaviour, which corresponds to that of $CoFe_2O_4$ nanoparticles. The toxicity evaluation of the synthesised HNPs on *Chlorella vulgaris* indicated that they can be applied to biomedical applications such as magnetic hyperthermia, photothermal therapy, drug delivery, bioimaging and biosensing.

Keywords: $CoFe_2O_4$/Au nanoparticles; toxicity; X-ray photoelectron spectroscopy; anion-exchange resin precipitation; hybrid nanoparticles; synthesis; magnetic hysteresis loops

1. Introduction

The design, synthesis and applications of hybrid nanoparticles (HNPs) are hot research topics in the field of nanotechnology. HNPs are important due to their multi-functionalities that are difficult to achieve by a simple mixture of individual components. Due to the combination of physical and chemical (magnetic, optical) properties of compound substances, they can be used in various fields, such as chemistry, physics, microelectronics, biotechnology, catalysis and medicine [1–5].

Recently, the use of magnetic HNPs in theranostics (combining therapeutic and diagnostic functions in one nanoobject) has remarkably increased [6-9]. When an external magnetic field is applied to magnetic nanoparticles, they can be directed to a specific area (organ or tissue) along with drug molecules attached to their surfaces [10-13].

Among various iron oxide-based nanomaterials, magnetite has been the most popular for biomedical applications. Additionally, it has the strongest magnetism among

Preprints (www.preprints.org) | NOT PEER-REVIEWED | Posted: 18 March 2021 doi:10.20944/preprints202103.0464.v1

iron oxides. However, magnetite nanoparticles exhibited toxicity in cell cultures and animal studies [14-15]. Additionally, magnetite is extremely sensitive to oxidation, decreasing its magnetic properties; thus, it requires a protective capping layer [16-17]. Cobalt and nickel ferrites are often considered as alternatives to magnetite [18-19]. These materials are attractive due to their high chemical stability and significant magnetism.

Due to recent advances in surface chemistry, nanoparticle functionalization has been tremendously developed. Gold is one of the most effective coating materials to protect magnetic nanoparticles and increase their biocompatibility. Additionally, the optical and catalytic properties of gold-coated magnetic nanoparticles can be varied by the type of coating (thick shell or decoration with nanoclusters) and the morphology and size of gold nanoparticles on the surface [20-22].

While numerous studies have demonstrated the production of hybrid gold-based nanoparticles, a reliable and predictable synthetic strategy that provides reproducibility has not been realized. There are two main approaches in the literature to synthesize these materials: In the first case, gold seeds with a diameter 1–3 nm are prepared by the reduction with borohydride [23] or sodium citrate [24]. Then, the obtained seeds are added to magnetic particles. The surface of the particles is pre-modified with biomolecules or polymers to attach gold nanoclusters. Polyethyleneimine (PEI) is a well-established agent for the surface treatment of magnetic nanoparticles [25-26]. Another technique involves creating an intermediate layer of silica dioxide with grafted amino groups of 3-aminopropyltrimethoxysilane (APTMS) or mercapto groups on the surface of magnetic nanoparticles [27-28]. However, it is often challenging to attach gold seeds onto the nanoparticle surface due to the large lattice mismatch between the magnetic material and gold.

Another approach is to form a surface complex with gold ions. The surface of the magnetic material is modified with bifunctional ligands, such as citrate [29, 30], dithiosuccinic acid [5] and methionine [31]. The bifunctional ligand must have a high affinity for both the magnetic nanoparticle and gold ions. Additionally, an excess ligand can act as a reducing agent. Additional reducing agents (ascorbic acid [32, 33], hydroxylamine [34]) may be used in this approach. However, gold is often not deposited on the NP surface but forms large particles (50–80 nm) in the solution. To control gold deposition, a reducing agent, modifier and stabiliser must be selected carefully.

We provide a simple, fast and easily reproducible method to obtain cobalt ferrite HNPs, where a strong-base anion-exchange resin in OH form is used as a precipitant of cobalt and ferric ions. During the process, anions in the solution (Cl^-) exchange with the OH- ions of the resin (Co^{2+}, Fe^{3+} and OH^- given off by the resin can combine to form hydroxides). This process is conducted under easily controllable stationary conditions and allows obtaining homogeneous nanoparticles with uniform size and morphology without impurity ions. This method eliminates the use of expensive equipment and multiple washing steps [35, 36]. The anion-exchange resin precipitation is conducted in the solution containing dextran-40 to prevent the aggregation of the as-obtained magnetic nanoparticles and control the particle size. As we have previously discussed [37], the formation of new nuclei dominates crystal growth due to steric stabilisation as a consequence of polymer adsorption on the surface of magnetic nanoparticles. In this study, we used L-methionine as a reducing agent, an anchor between $CoFe_2O_4$ and gold and a stabilising agent for nanoparticles. The gold deposition on the surface of $CoFe_2O_4$ cores with methionine was performed in several cycles.

2. Materials and Methods

2.1. Chemicals

Cobalt chloride ($CoCl_2 \cdot 6H_2O$), iron chloride ($FeCl_3 \cdot 6H_2O$), tetrachloroauric(III) acid ($HAuCl_4$), L-methionine ($CH_3SCH_2CH_2CH(NH_2)CO_2H$), dextran (($C_6H_{10}O_5$)n Mr ~40000 g/mol) and other chemicals were of analytical grade, purchased from Sigma-Aldrich, and used as received. The strong-base anion-exchange resin AV-17-8 with a polystyrene gel matrix was produced by "Azot" Corporation (Cherkassy, Ukraine) in the chloride form

Preprints (www.preprints.org) | NOT PEER-REVIEWED | Posted: 18 March 2021 doi:10.20944/preprints202103.0464.v1

with a bead size of 0.4−0.6 mm (Russian GOST 20301-74). This resin has a gel matrix based on polystyrene cross-linked with divinylbenzene and functional group quaternary ammonium (type I). This resin is an analogue of Purolite A400/A300, Lewatit M-500, Amberlite IRA 402/420, Dowex SBR-P/ Maraton A, has a significantly lower cost and is widely used in separation, purification and decontamination processes in Russia.

2.2. Synthesis of cobalt ferrite nanoparticles

The proposed approach differs from the reported one [38] in the nature and of magnetic NPs, the technique of their production, the concentration of the aqueous solution applied and synthesis modes. In this study, cobalt ferrite nanoparticles were synthesised by anion-exchange resin precipitation. The synthesis procedure was described in detail in [37]. Briefly, $CoCl_2 \cdot 6H_2O$ (1.2 g) and $FeCl_3 \cdot 6H_2O$ (3.4 g) were dissolved in dextran-40 (50 mL, 10%) to stabilise the colloidal system and reduce the particle size. Excess AV-17-8(OH) (150 %) is added to a solution containing cobalt and ferric salts. The mixture was stirred (180 rpm) at a temperature of 60 °C using a magnetic stirrer for 1 h. To remove the anion-exchange resin beads from the reaction products, a sieve with round holes (0.16 mm in diameter) was used; the precipitate was centrifuged, washed with distilled water, dried in air at 80 °C and then annealed in a muffle furnace at 600°C for 1 h.

2.3. Synthesis of hybrid $CoFe_2O_4$/Au nanoparticles

Hybrid $CoFe_2O_4$/Au nanoparticles were fabricated by methionine-directed gold deposition from $HAuCl_4$ solution according to a modified technique described in [31]. Cobalt ferrite nanoparticles (25 mg) were dispersed in L-methionine (20 mL, 0.03 mol/L) by ultrasonic agitation (ultrasonic bath "Sapphire") for 30 min. Chlorauric acid (20 mL, 0.6 mmol/L) was added to the mixture; pH was adjusted to ten by the addition of NaOH (1 mol/L). The deposition process was conducted at 37 °C for 4 h under stirring (800 rpm). The resulting nanoparticles were separated by magnetic separation and thoroughly washed with distilled water and ethanol. The procedure of gold deposition was repeated up to ten times under the same conditions. The nanoparticles after one, six and ten deposition cycles were collected for characterisation.

2.4. Nanoparticle characterisation

The phase composition of samples was determined on a Shimadzu XDR-600 (Shimadzu Corporation, Kyoto, Japan) diffractometer employing monochromatic CuKα radiation; phase identification was performed according to the JCPDS Powder Diffraction File №22-1086. TEM, EDX analysis, and selected area electron diffraction characterisation were carried out using Hitachi 7700M (Hitachi Corporation, Hitachi, Japan, the accelerating voltage: 110 kV) and JEM 2100 (JEOL, Japan) transmission electron microscope operated at an accelerating voltage of 200 kV. A cobalt ferrite particle size distribution histogram was obtained from more than 300 particles. UV-vis absorption spectra were collected in a glass cell with an optical path of 1 cm employing a GENESYS 10S UV-Vis Spectrophotometer (Thermo Scientific, Bedford, USA). The FTIR spectra of samples were recorded on a Tensor 27 (Bruker, Germany) FTIR spectrometer in the range 4000–400 cm^{-1}. XPS studies were performed using a hydrosol dried with highly oriented pyrolytic graphite (HOPG) and gently rinsed with water. The spectra were acquired using a SPECS spectrometer (SPECS Gmbh, Germany) equipped with a PHOIBOS 150-MCD-9 hemispherical electron analyser. Spectra were recorded upon excitation with monochromatic radiation of AlKα (E = 1486.6 eV) and MgKα (E = 1253.6 eV). The analyser pass energy was 10 eV for high-resolution scans and 20 eV for survey spectra. An electron flood gun was applied to eliminate inhomogeneous electrostatic charging of the samples; the C 1s peak at 284.45 eV from HOPG was used as a reference. The high-resolution spectra were fitted after the subtraction of Shirley-type background with Gaussian–Lorentzian peak profiles using CasaXPS software (version 2.3.16, Casa Software, Teignmouth, UK). Magnetic properties of the material obtained were investigated using a vibrating sample

Preprints (www.preprints.org) | NOT PEER-REVIEWED | Posted: 18 March 2021 doi:10.20944/preprints202103.0464.v1

and SQUID magnetometers in a magnetic field up to ±10 kOe at 298 K. An electromagnet with high magnetic field uniformity was used as a source. Magnetic measurements were performed using a direct method of measuring the inductive electromotive force. Mechanical vibrations of the sample were provided by a vibrator of the original design. The relative instability of the oscillation amplitude was 0.01% with a frequency of 0.001%. Registration of the signal was conducted using the system of four pickup coils. The dynamic range of the device was 5.10−6–100 emu. The toxicity of the nanoparticles was studied on an algologically clean test culture of Chlorella vulgaris Beijer in the exponential stage of growth. The experiment was carried out in a multi-cell cultivator KVM-05 (Russia, Europolytest) in four parallels. The microalgae species were cultivated at a medium temperature of 36 °C, light irradiation with an average intensity of 60 W/m^2 and CO_2 provision from the air (0.03%). 24 samples of microalgae species in 2% nutrient medium of Tamiya (6 cm^3) were placed into cuvettes (10 cm^3). Nanoparticles were introduced into the cultivation water in concentrations of 0.08, 0.46, 2.78, 3.13, 6.25, 12.50, 16.67 and 25 mg/l. The viability of the test culture (equation (1)) in the sample medium was determined by the change in optical density relative to the reference using spectrometer IPS-03 (Russia, Europolytest) equation (1):

$$\text{Viability} = (1 - (D_R - D_{EXP})/D_R) \cdot 100\%, \quad (1)$$

where D_R and D_{EXP} are average values of optical density in the reference and the experiment, respectively.

3. Results

Cobalt ferrite nanoparticles were synthesized using anion-exchange resin precipitation based on the ion exchange between the anions of the aqueous solution and a solid substance (an anion-exchange resin, containing the OH groups). The co-precipitation of $Co(OH)_2$ and $Fe(OH)_3$ can be described by equation (2):

$$5R\text{-}OH + CoCl_2 + FeCl_3 \rightarrow 5R\text{-}Cl + Co(OH)_2\downarrow + Fe(OH)_3\downarrow, \quad (2)$$

where R-OH, R-Cl – anion-exchange resin AV-17-8 with OH- and Cl- groups on the resin substrate, respectively.

The precipitation of metal hydroxides occurs at the resin–solution interface, namely on the resin beads. When the thickness of the surface deposit reaches 1–1.5 μm, it is exfoliated, and an individual product phase forms [35, 36]. We used a polysaccharide, dextran-40, to obtain homogeneous nanoparticles with similar sizes and morphologies. According to [37], dextran-40 adsorbs on the primary hydroxide particles and protects against coalescence and/or aggregation.

Thus, the precipitate obtained is free from impurity ions because no additional reagents besides the anion-exchange resin are used, and the anions of the initial salts are trapped by polymer beads. Accordingly, the product does not require multiple washing steps. The product annealed for 1 h at 600°C was investigated by X-Ray diffraction (XRD) (Figure 1a). The position and relative intensity of all diffraction peaks match well with the standard $CoFe_2O_4$ diffraction data JCPDS №22-1086. The average crystallite size determined from the peak broadening for the four most intense XRD peaks using the Scherrer equation (equation (3)) was 12.4 ± 1.0 nm. This result is in a good agreement with transmission electron microscopy (TEM) characterization, which shows that the obtained nanoparticles have a narrow particle size distribution and a size range 10–20 nm.

$$D = (b \cdot \lambda)/(FWHM \cdot \cos\Theta), \quad (3)$$

where FWHM is the full width at the half-maximum intensity of the peak, 2θ is the scattering angle in radians, λ is the wavelength (1.5406 Å), b is a constant, which is a function of the crystallite geometry, and is taken between 0.89 and 0.94, and D is the average size of crystallites.

Preprints (www.preprints.org) | NOT PEER-REVIEWED | Posted: 18 March 2021 doi:10.20944/preprints202103.0464.v1

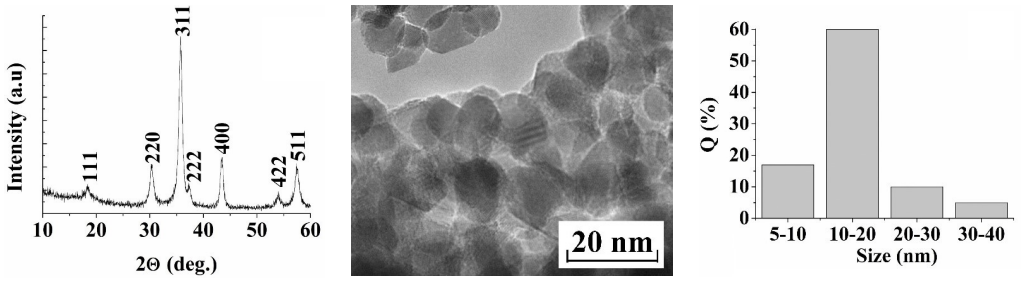

Figure 1. (a) XRD pattern, (b) TEM image and (c) size distribution histogram of cobalt ferrite particles synthesised by anion-exchange resin co-precipitation in a solution of $FeCl_3$, $CoCl_2$ and 10 % dextran-40 at 60 ˚C and annealed at 600 ˚C for 1 h.

To obtain hybrid nanoparticles based on cobalt ferrite and gold, we modified the technique reported in [31]. This technique includes several stages. The first step is to treat cobalt ferrite nanoparticles by L-methionine. Then, the hydrogen tetrachloroaurate (III) and NaOH solutions are added. As a result, the seeds of Au^0 are deposited on the ferrite nanoparticle surface during reduction by L-methionine without using other reducing agents. The L-methionine and $H[AuCl_4]$ treatments of the nanoparticles are numerously repeated.

Figure 2 shows FTIR absorption spectra of the cobalt ferrite nanoparticles before (curve 1) and after (curve 2) their treatment by L-methionine. The spectra of both samples are similar and contain the absorption bands at 590 and 450 cm^{-1}, which are typical for cobalt ferrite and correspond to the stretching vibrations of metal-oxygen bonds. The weak absorption bands at 3400 cm^{-1} is due to the stretching vibrations of OH groups and the deformation vibrations of water molecules adsorbed on the surface of $CoFe_2O_4$ nanoparticles. In the range 1800–1200 cm^{-1} of the spectrum of sample 2, a few weak lines corresponding to the deformation vibrations of NH_3^+ (1508 cm^{-1}), asymmetric and symmetric vibrations of COO^- groups (1581 and 1402 cm^{-1}), scissoring vibration H_2O (1622 cm^{-1}) and deformation vibration of CH_3 groups (1346 cm^{-1}) of methionine were observed [39]. The low intensities of these peaks indicate the weak adsorption of methionine on the surface of cobalt ferrite nanoparticles after one cycle of treatment by L-methionine. The frequencies of $\nu s(COO^-)$ and $\delta(NH_3^+)$ downshift slightly (from 1414 to 1402 cm^{-1} and from 1515 to 1508 cm^{-1} respectively) upon treatment of ferrite NPs with methionine molecules. Such frequency downshifts may be due to the interaction of COO^- and NH_3^+ groups of the amino acid with the surface of cobalt ferrite nanoparticles [31]. Nevertheless, it was observed only insignificant sorption of the methionine molecules on NPs, therefore, the nature of the bonding between amino acid and $CoFe_2O_4$ requires additional research.

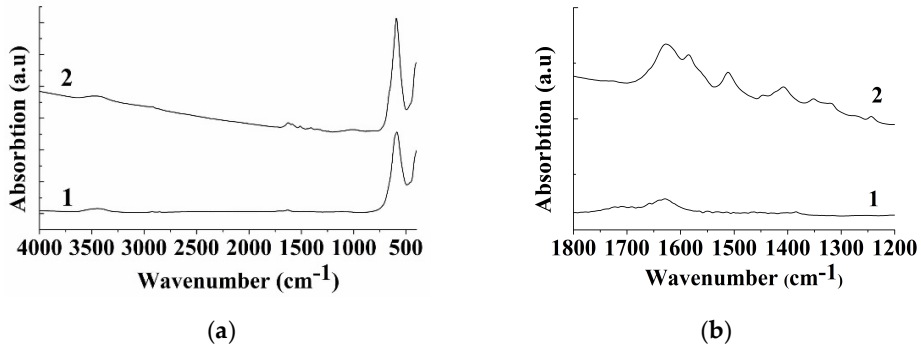

Figure 2. FTIR spectra of cobalt ferrite nanoparticles in the spectral regions of 4000−500 cm^{-1} (a) and 1800 − 1200^{-1} cm^{-1} (b) syntheScheme 3. $CoCl_2$ and 10 % dextran-40 at 60 ˚C and annealed at 600 ˚C for 1 h before (1) and after (2) treatment by methionine (20 mL, 0.03 mol/L).

Preprints (www.preprints.org) | NOT PEER-REVIEWED | Posted: 18 March 2021 doi:10.20944/preprints202103.0464.v1

Figure 3 shows the TEM images of hybrid $CoFe_2O_4$/Au nanoparticles after one, six and ten cycles of gold deposition. We can see small gold clusters on the cobalt ferrite nanoparticles, as confirmed by the energy-dispersive X-ray spectroscopy (Figure 4). The size of the gold nanoclusters slightly increases with an increase in the number of gold deposition cycles: 2.12 ± 0.15 nm for one cycle, 2.15 ± 0.15 nm for six cycles and 2.46 ± 0.13 nm for ten cycles. However, we shall notice that the density of the gold nanoclusters on the cobalt ferrite surface does not change with the increase in the number of gold deposition cycles.

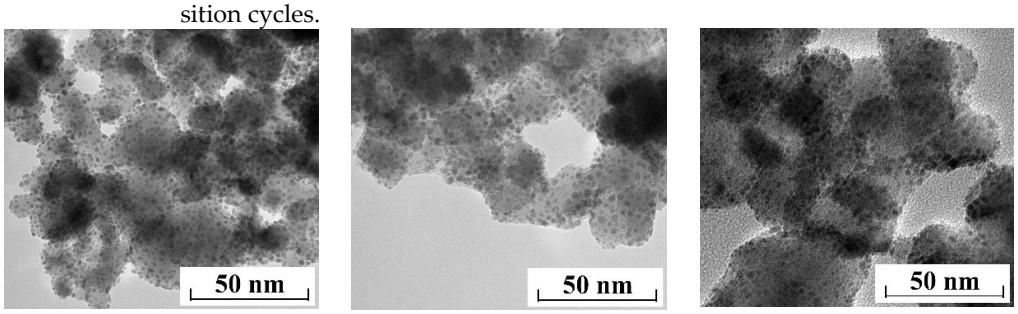

Figure 3. TEM images of $CoFe_2O_4$/Au nanoparticles after gold deposition from the alkaline (pH = 12) solution containing 0.03 mol/L HAuCl4 and 0.03 mol/L methionine at 37°C for 4 h: (a) 1 gold deposition cycle, (b) 6 gold deposition cycles and (c) 10 gold deposition cycles.

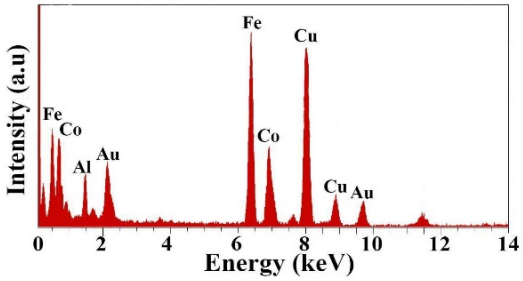

Figure 4. Energy-dispersive X-ray spectrum of $CoFe_2O_4$/Au nanoparticles after 6 gold deposition cycles.

The obtained after 1 gold deposition cycle particles redispersed in ethanol and the solution remaining after separation of the magnetic particles were studied by a spectrophotometer in the wavelength range of 400–1000 nm. Dispersed $CoFe_2O_4$/Au NPs show an absorption peak at 580 nm (Figure 5). The shift of the characteristic peak for Au NPs (520 nm) is a consequence of their adsorption on the surface of cobalt ferrite nanoparticles [40]. The optical density of the solution after the magnetic separation of nanoparticles is much lower than in the initial hydrosol and may be due to the residual amount of nanoparticles. This indicates that the reduction of gold occurs on the surface of the cobalt ferrite and not in the volume of the solution.

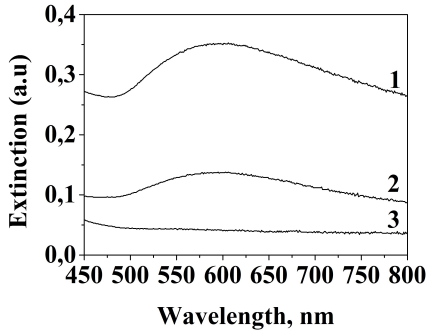

Preprints (www.preprints.org) | NOT PEER-REVIEWED | Posted: 18 March 2021 doi:10.20944/preprints202103.0464.v1

Figure 5. Optical absorption spectra of $CoFe_2O_4$ nanoparticles before (3) and after (1) 1 gold deposition cycle from the alkaline (pH = 12) solution containing 0.6 mmol/L $HAuCl_4$ and 0.03 mol/L methionine at 37 °C for 4 h, and spectra of solution (2) remaining after $CoFe_2O_4$/Au nanoparticles (NPs) magnetic separation.

X-ray photoelectron spectroscopy (XPS) was applied to study the surface composition and chemical state of elements in the hybrid nanoparticles $CoFe_2O_4$/Au obtained after one, six, and ten gold deposition cycles. The survey spectra (Figure 6) contain the peaks Au 4f, S 2p, O 1s, N 1s, C 1s, Fe 2p and Co 2p. The presence of Fe 2p and Co 2p in all spectra indicates that a solid gold shell was not formed, even after 10 gold deposition cycles. The surface chemical composition of the $CoFe_2O_4$/Au NPs is presented in Table 1. The concentration of gold on the NPs surface decreases with an increase in the number of deposition cycles. We suppose that the partial desorption of adsorbed gold nanoparticles is caused by additional steps of the sonication treatment, magnetic separation and washing of $CoFe_2O_4$/Au NPs during extra gold deposition cycles.

The N/S atomic ratios obtained from XPS spectra of all the samples ranged from 0.7 to 0.8. This indicates the presence on the surface of the obtained nanoparticles adsorbed methionine as well as the product of its oxidation by Au^{3+} that is believed to be methionine sulfoxide CH_3-S(O)$CH_2CH_2C(NH_2)COOH$ [41].

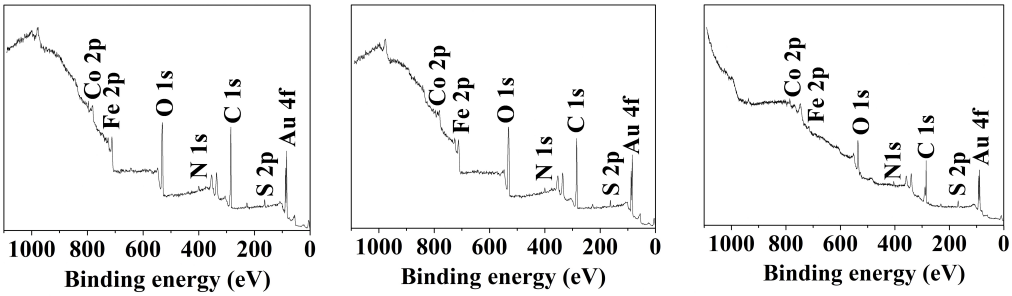

Figure 6. Wide XPS spectra of $CoFe_2O_4$/Au synthesized under the conditions in Figure 3: (a) 1 gold deposition cycle, (b) 6 gold deposition cycles and (c) 10 gold deposition cycles.

Preprints (www.preprints.org) | NOT PEER-REVIEWED | Posted: 18 March 2021 doi:10.20944/preprints202103.0464.v1

Table 1. Elemental composition of $CoFe_2O_4$/Au NPs.

Name	Peak BE, eV	Atom, % Number of gold deposition cycles		
		1	6	10
Au 4f	83.9	5.1	3.5	3.1
C 1s	284.6	62.1	57.3	57.5
N 1s	399.6	2,5	2.7	2.2
O 1s	530.2	26.0	27.6	29.2
Fe 2p	710.8	0.8	3.3	3.1
Co 2p	780.6	1.4	2.1	2.4
S 2p	162.8	4.6	3.4	2.6

To gain a better insight into the chemical state of sulfur at the surface of $CoFe_2O_4$/Au the narrow XPS spectra for S 2p were recorded (Figure 7). The spectrum S 2p (Figure 7a) of the hybrid nanoparticles was obtained after one cycle of gold deposition shows a doublet with a binding energy S $2p_{3/2}$ 162.6 eV. The energies of the peaks in the spectrum are similar to those of methionine [38] and can be assigned to the thioether group C-S-C [42,43].

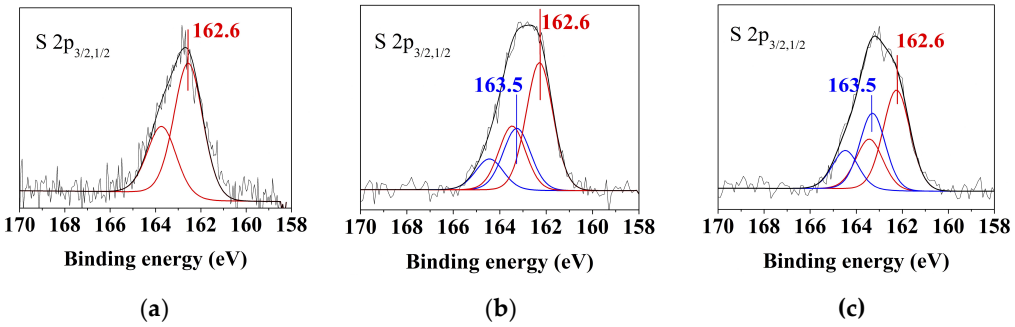

Figure 7. Spectra of S 2p XPS of $CoFe_2O_4$/Au nanoparticles synthesized under the conditions in Figure 3: (a) 1 gold deposition cycle, (b) 6 gold deposition cycles and (c) 10 gold deposition cycles.

As the number of the gold deposition cycles increase (Figure 7b, c) the major doublet S 2p does not change their position; however, a second minor doublet with the binding energy S $2p_{3/2}$ of 163.5 appears in the spectra. This doublet can be attributed to the product of methionine oxidation. The lines with $S2p_{3/2}$ binding energies of 163.5, which are typically assigned to polysulfide species, were observed in the XPS spectra of core-shell $NiFe_2O_4$@Au nanoparticles obtained by the reduction of gold with methionine [38]. These results indicate the dimerization of methionine during its oxidation with the formation of two-centre three-electron (2c–3e) S–S bonds [44].

The spectra of Au $4f_{7/2,5/2}$ $CoFe_2O_4$/Au nanoparticles obtained after one cycle of gold deposition (Figure 8a) can be fitted to three components. The major doublet of the Au $4f_{7/2}$ peak with a binding energy of 84,9 eV corresponds to Au^+ species, the component at 84.0 eV is due to metallic Au, and the third doublet of Au $4f_{7/2}$ with a binding energy of 85,6 eV corresponds to Au(III). The presence of Au (III) in the spectra can be explained by the fact that $[AuCl_2]^-$ disproportionates exceptionally quickly in aqueous solutions, forming $[AuCl_4]^-$ and metallic gold (equation (4)).

$$3[AuCl_2]^- = 2Au^0 + [AuCl_4]^- + 2Cl^- \quad (4)$$

Preprints (www.preprints.org) | NOT PEER-REVIEWED | Posted: 18 March 2021 doi:10.20944/preprints202103.0464.v1

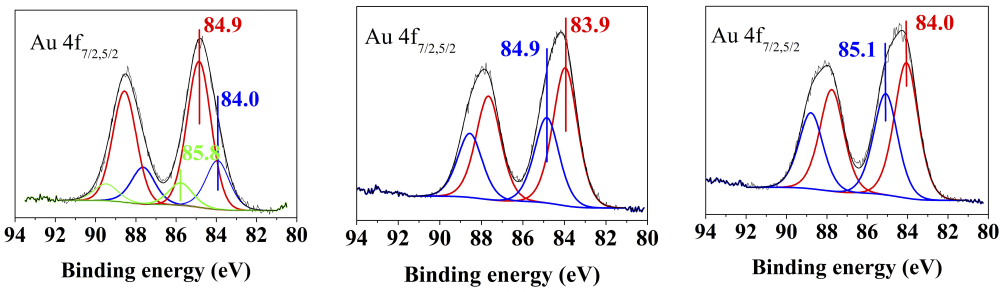

Figure 8. Spectra of Au 4f XPS of CoFe2O4/Au nanoparticles synthesized under the conditions in Figure 3: (a) 1 gold deposition cycle, (b) 6 gold deposition cycles and (c) 10 gold deposition cycles.

The spectra of Au 4f of $CoFe_2O_4$/Au nanoparticles obtained after 6 and 10 cycles of gold deposition (Figure 8b,c) can be decomposed into two components: Au^0 and Au^+ with binding energies given in Table 2. The increase in the number of deposition cycles from one to six leads to almost a two-fold increase in Au^0 concentration and a two-fold decrease in Au^+ concentration. If the number of cycles rises further, the concentrations of the Au species on the surface of the hybrid nanoparticles stay the same. The presence of Au (I) spectral lines can be explained by the adsorption of $[AuCl_2]^-$ or gold (I) sulphide on the surface of nanoparticles and should be investigated further.

Table 2. Relative concentrations of Au species derived from XPS analysis (At. %) and binding energy of Au $4f_{7/2}$ peak.

The number of gold deposition cycles	Au(0)		Au(I)		Au(III)	
	%	Pos., eV	%	Pos., eV	%	Pos., eV
1	7,3	84,0	22,6	84,9	3,6	85,8
6	14,3	83,9	8,9	84,9	-	-
10	13,4	84,0	10,0	85,1	-	-

Figure 9 shows the dependance of the magnetisation of the nanoparticles before and after one cycle of gold deposition on the applied magnetic field measured at 298 K. The values of the saturation magnetisation (Ms) were estimated in magnetic field H = 10 kOe. The specific residual magnetisations (Mr) were determined from the point of intersection of the drop-down portion of the magnetisation curve with the Y-axis. The values of coercivity (Hc) of the nanoparticles were determined by the measurement of the hysteresis loop width. The basic parameters of the hysteresis loops are collected in Table 3.

Table 3. Magnetic parameters obtained from the results of magnetic hysteresis loops in Figure 9.

Sample	Ms, emu/g	Mr, emu/g	Hc, Oe
$CoFe_2O_4$	33.21	7.55	510
$CoFe_2O_4$/Au	27.04	6.31	600

Preprints (www.preprints.org) | NOT PEER-REVIEWED | Posted: 18 March 2021 doi:10.20944/preprints202103.0464.v1

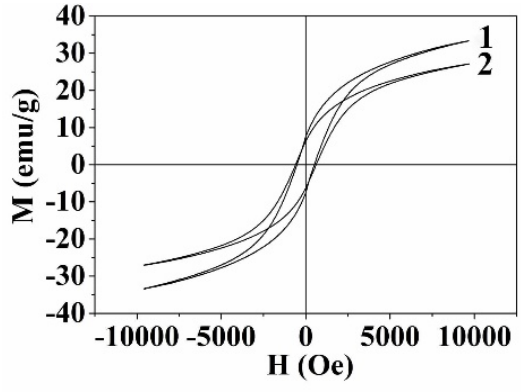

Figure 9. Magnetisation curves of $CoFe_2O_4$ (1) before and (2) after one gold deposition cycle measured in magnetic field H = ±10 kOe at 298 K.

The results show ferrimagnetic behaviour of both samples. The magnetic moments of various sublattices of ferrimagnetics including cobalt ferrite are oriented antiparallel, but the magnitudes of their magnetic moments are not equal. As a result, the resulting magnetic moment is not equal to zero. The magnetic moments of octahedrally coordinated Co^{2+} ions are uncompensated, whereas the magnetic moments of Fe^{3+} ions are fully compensated due to the ionic spin of the octahedrally coordinated Fe^{3+} ions being oriented opposite to the spins of the tetrahedrally oriented ions. In ferrimagnets, magnetic ordering is retained in the absence of an external field (the magnetising effect).

The observed saturation magnetisation values (33.21 emu/g $CoFe_2O_4$ and 27.04 emu/g for $CoFe_2O_4$/Au) are noticeably lower than the bulk values (80.8 emu/g) [45]. It is known that decreasing the particle size decreases the saturation magnetisation of the material. It is generally attributed to increasing surface spin canting caused by the structural disorder of surface atoms [46]. Decreasing the particle size leads to an increase in the relative number of atoms in the surface layer.

An insignificant decrease in the magnetic saturation and residual magnetisation values per mass of the sample was observed for $CoFe_2O_4$/Au due to the presence of diamagnetic gold. However, the coercive force of this sample increases slightly. We argue that this is primarily due to the loss of small gold-ferrite particles during additional washing and magnetic separation.

The magnetic properties strongly depend on the prehistory of the sample (annealing, preparation method, size and morphology of crystallites) [47]. The values of the magnetic parameters of $CoFe_2O_4$ nanoparticles reported in the literature vary from Ms ~15–20 [48, 49] to 60–70 emu/g [46, 50].

The cytotoxicity of the obtained HNPs remains an important issue to realise its potential applications in biology and medicine. The unicellular green algae *Chlorella vulgaris* was used as a test organism in our experiments. This alga is a widely used test object; it can be grown in a synthetic medium and multiplies rapidly. The survival of the test organism depends on the concentration of nanoparticles for both $CoFe_2O_4$ and $CoFe_2O_4$/Au nanoparticles obtained after one cycle of gold deposition. We found that gold-containing nanoparticles with a non-continuous gold shell showed lower toxicity compared to bare $CoFe_2O_4$ nanoparticles. At a nanoparticle concentration of 25 mg / L, the 85% viability of the test culture in the presence of $CoFe_2O_4$/Au was higher compared to that (40%) in the case of bare $CoFe_2O_4$ nanoparticles (Figure 10).

Preprints (www.preprints.org) | NOT PEER-REVIEWED | Posted: 18 March 2021 doi:10.20944/preprints202103.0464.v1

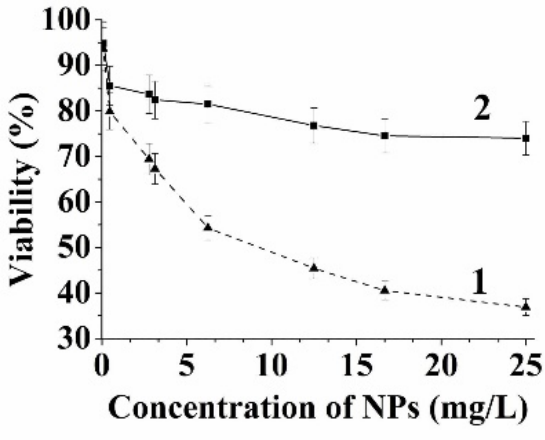

Figure 10. Cell viability of test culture of Chlorella vulgaris Beijer in the environment of CoFe2O4 nanoparticles (1) before and (2) after one gold deposition cycle.

To obtain magnetic nanoparticles suitable for biomedical applications, we used sulfur-containing amino acid L-methionine as both a biocompatible reducing agent and an anchor between $CoFe_2O_4$ and gold. L-methionine plays an important role in metabolism, methylation and transmethylation reactions in organisms [51-53], as well as metal bonding in the structure of many enzymes [54, 55]. It is known that methionine is one of the few reducing amino acids. Moreover, as shown in [31,38], methionine does not form separate gold crystals in the solution bulk, reducing unwanted side reactions and gold waste.

While many studies have been conducted on the topic, the mechanism of the methionine oxidation by $[AuCl_4]^-$ ions is not completely clear. According to [41, 56-58], the reaction occurs in two steps. At the first step, methionine rapidly coordinates as a bidentate S- and N-donor ligand with Au (III) ion and forms an intermediate complex $[AuCl_2(HMet)]^{2+}$ (for acidic solutions) or $[AuCl_2(Met)]^+$ (for alkaline solutions). At the second step, the intermediate reacts with the second methionine molecule to form methionine sulfoxide as a product of methionine oxidation and the hydrolysis of the intermediate compound. $[AuCl_2]^-$ formed during the process then disproportionates, forming $[AuCl_4]^-$ and metallic gold. However, other oxidation routes are also possible. In the Scuderi's research [59] and Asmus's work [60,61], the methionine oxidation process is complex and influenced by many conditions, and sulfoxide is not the sole product as it has been shown earlier. The ammonia and CO_2 were found by Scuderi among the oxidation products of methionine, which indicates the decarboxylation and deamination of the amino acid. Additionally, the dimerisation of methionine (or its decomposition product) occurs during the oxidation process with the formation of a two-centre three-electron S-S bond (2c-3e), as noted by many researchers [44, 62, 63]. According to the XPS data, we observed this product during the deposition of gold on the surface of the nanoparticles. Moreover, its concentration increases with an increasing number of gold deposition cycles. This finding has been obtained earlier in our research [38].

As discussed above, in this paper, 10–15-nm magnetic nanoparticles of cobalt ferrite decorated with 2-nm gold nanoclusters have been obtained. It is worth noting that the nanomaterials decorated with gold are of interest for catalytic applications [64, 65]. The gold-decorated nanoparticles were synthesised by Félix et al. [22] using polyethyleneimine-treated Fe_3O_4 as magnetic cores and sodium borohydride as a reducing agent, and by Silvestri et al. [5] using $CoFe_2O_4$ and 2,3-meso-dimercapto succinic acid as a bifunctional organic ligand.

In contrast to our previous study [38], a continuous gold shell on the surface of the $CoFe_2O_4$ nanoparticles was not formed, even after ten cycles of gold deposition. The obtained results showed only a minor increase in the size of gold nanoclusters: from 2.12 ± 0.15 nm to 2.46 ± 0.13 nm with the number of the nanoclusters remaining unchanged

 doi:10.20944/preprints202103.0464.v1

during multiple repeats. The supernatant solutions obtained after the synthesis were transparent and colourless, indicating the absence of gold nanoparticles in the solution. Further, methionine reduces gold only on the surface of cobalt ferrite nanoparticles, not in the solution. We speculate that future studies should include using an additional reducing agent stronger than methionine to form the gold shell on the magnetic core surface. In [66], to obtain core-shell nanoparticles, formaldehyde as an initiator of gold deposition on the surface of silicon dioxide was used. Goon et al. [67] grew gold shell on Fe_3O_4 - polyethyleneimine–Au seed by the iterative reduction of $HAuCl_4$ with $NH_2OH{\cdot}HCl$.

Despite the absence of a solid gold shell, the toxicity of the hybrid $CoFe_2O_4$/Au nanoparticles greatly reduced even after one cycle of gold deposition. The obtained nanomaterial shows ferrimagnetic behaviour. When ferrimagnetic nanoparticles are placed in external alternating magnetic fields, they can rapidly be heated due to the absorption of the electromagnetic field energy [68]. We believe this feature coupled with low toxicity makes $CoFe_2O_4$/Au nanoparticles suitable candidates for potential applications in magnetothermal therapy. Additionally, such particles can be easily directed to certain organs and tissues together with drug molecules attached to their surface with the help of an external magnetic field.

4. Conclusions

The synthesis of magnetic $CoFe_2O_4$/Au HNPs from cobalt ferrite and $H[AuCl_4]$ using L-methionine was demonstrated. Cobalt ferrite nanoparticles with a size range 10–20 nm as magnetic cores were prepared by a simple, fast and easily reproducible method, where the strong-base anion-exchange resin in OH form was used as a precipitant of cobalt and ferric ions. To attach gold to the $CoFe_2O_4$ surface, direct reduction of Au(III) by methionine, which also acts as an anchor between the nanoparticle surface and gold, was performed. The gold deposition was repeated up to ten times under the same conditions. The formation of the hybrid $CoFe_2O_4$/Au particles was analysed by XPS. The TEM images of the HNPs obtained after one, six and ten gold deposition cycles showed that the surface of cobalt ferrite was covered with gold nanoclusters, which slightly increased with an increase in the number of gold deposition cycles (from 2.12 ± 0.15 nm after one cycle to 2.46 ± 0.13 nm after ten cycles) without any change in surface density. A continuous gold shell on the surface was not formed, even after ten gold deposition cycles. We assume that an additional reducing agent stronger than methionine should be used to form the gold shell on the magnetic core surface.

In accordance with the magnetometry data, $CoFe_2O_4$/Au nanoparticles demonstrate ferrimagnetic behaviour (Ms = 27.04 emu/g, Hc = 600 Oe at 300 K) corresponding to that for bare cobalt ferrite nanoparticles. The comparative study of the toxicity of the synthesised HNPs on a test organism of the unicellular green alga *Chlorella vulgaris* showed that the toxic effect of $CoFe_2O_4$/Au nanoparticles obtained was noticeably reduced, even after one gold deposition cycle, compared to that of uncoated cobalt ferrite nanoparticles. The low toxicity and suitable magnetic properties of $CoFe_2O_4$/Au nanoparticles make them potential candidates for applications in magnetothermal therapy.

Author Contributions: Conceptualization, S.S., A.P., T.T. and D.K.; Formal analysis, S.S., A.P., T.T.; D.K and Y.M.; Investigation, A.P., T.T.; Y.M., D.K.; A.A., Y.G., M.V., S.Z. and D.V.; Methodology, S.S.; Supervision, S.S.; Validation, S.S.; Writing—original draft, S.S., A.P. and T.T.; Writing—review & editing, Y.M. All authors have read and agreed to the published version of the manuscript.

Funding: This research received no external funding.

Acknowledgments: The authors thank the Federal Research Center "Krasnoyarsk Science Center of the Siberian Branch of the Russian Academy of Sciences" for using its facilities.

Conflicts of Interest: The authors declare no conflict of interest.

References

1. Sanchez, L.M.; Alvarez, V.A. Advances in magnetic noble metal/iron-based oxide hybrid nanoparticles as biomedical devices. *Bioengineering* **2019**, 6, 75.
2. Wang, H.; Shen, J.; Li, Y.; Wei, Z.; Cao, G; Hong, K.; Banerjee, P.; Zhou, S. Porous carbon protected magnetite and silver hybrid nanoparticles: morphological control, recyclable catalysts, and multicolor cell imaging. *ACS Appl. Mater. Interfaces* **2013**, 5, 9446-9453.
3. Lu, L.; Hao, Q.; Lei, W.; Xia, X.; Liu, P.; Sun, D.; Wang, X.; Yang, X. Well-Combined Magnetically Separable Hybrid Cobalt Ferrite/Nitrogen-Doped Graphene as Efficient Catalyst with Superior Performance for Oxygen Reduction Reaction. *Small* **2015**, 11, 5833-5843.
4. Saire-Saire, S.; Barbosa, E.C.M.; Garcia, D.; Andrade, L.H.; Garsia-Segura, S.; Camargo, P.H.C.; Alarcon, H. Green synthesis of Au decorated CoFe2O4 nanoparticles for catalytic reduction of 4-nitrophenol and dimethylphenylsilane oxidation. *RSC Adv.* **2019**, 9, 22116-22123.
5. Silvestri, A.; Mondini, S.; Mareli, S.; Prifferi, V.; Faciola, L.; Ponti, A.; Ferretti, A.M.; Poloto, L. Synthesis of water dispersible and catalytically active gold-decorated cobalt ferrite nanoparticles. *Langmuir* **2016**, 32, 7117-7126.
6. Efremova, M.V.; Nalench, Y.A.; Myrovali, E.; Garanina, A.S.; Grebennikov, I.S.; Gifer, P.K.; Abakumov, M.A.; Spasova, M.; Angelakeris, M.; Savchenko, A.G.; Farle, M.; Klyachko, N.L.; Majouga, A.G.; Wiedwald, U. Size-selected Fe3O4–Au hybrid nanoparticles for improved magnetism-based theranostics. *Beilstein J. Nanotechnol.* **2019**, 9, 2684-2699.
7. Yoo, D.; Lee, J.-H.; Shin, T.-H.; Cheon, J. Theranostic magnetic nanoparticles. *Acc. Chem. Res.* **2011**, 44, 863-874.
8. Reichel, V.E.; Matuszak, J.; Bente, K.; Heil, T.; Kraupner, A.; Dutz, S.; Cicha, I.; Faivre, D. Magnetite-Arginine Nanoparticles as a Multifunctional Biomedical Tool. *Nanomaterials* **2020**, 10, 2014.
9. Mohapatra, S.; Rout, S.R.; Das, R.K.; Nayak, S.; Ghosh, S.K. Highly hydrophilic luminescent magnetic mesoporous carbon nanospheres for controlled release of anticancer drug and multimodal imaging. *Langmuir* **2016**, 32, 1611-1620.
10. Jat, S.K.; Selvaraj, D.; Muthiah, R.; Bhattacharjee, R.R. A Self-Releasing Magnetic Nanomaterial for Sustained Release of Doxorubicin and Its Anticancer Cell Activity. *ChemistrySelect* **2018**, 3, 13123-13131.
11. Shima; Damodaran, P. Mesoporous Magnetite Nanoclusters as Efficient Nanocarriers for Paclitaxel Delivery. *ChemistrySelect* **2020**, 5, 9261-9268.
12. Oh, Y.; Moorthy, M.S.; Manivasagan, P.; Bharathiraja, S.; Oh, J. Magnetic hyperthermia and pH-responsive effective drug delivery to the sub-cellular level of human breast cancer cells by modified CoFe2O4 nanoparticles. *Biochimie* **2017**, 133, 7-19.
13. Mohapatra, S.; Rout, S.R.; Maiti, S.; Maitib, T.K.; Panda, A.B. Monodisperse mesoporous cobalt ferrite nanoparticles: synthesis and application in targeted delivery of antitumor drugs. *J. Mater. Chem.* **2011**, 21, 9185-9193.
14. Zhao, Z.; Huang, D.; Yin, Z.; Chi, X.; Wang, X.; Gao, J. Magnetite nanoparticles as smart carriers to manipulate the cytotoxicity of anticancer drugs: magnetic control and pH-responsive release. *J. Mater. Chem.* **2012**, 22, 15717-15725.
15. Ebadi, M.; Buskaran, K.; Bullo, S.; Hussein, M.Z.; Fakurazi, S.; Pastorin, G. Synthesis and Cytotoxicity Study of Magnetite Nanoparticles Coated with Polyethylene Glycol and Sorafenib–Zinc/Aluminium Layered Double Hydroxide. *Polymers* **2020**, 12, 2716.
16. Odio, O.F.; Lartundo-Rojas, L.; Santiago-Jacinto, P.; Martínez, R.; Reguera, E. Sorption of gold by naked and thiol-capped magnetite nanoparticles: an XPS approach. *J. Phys. Chem. C* **2014**, 118, 2776-2791.
17. Bui, T.Q.; Ngo, H.T.M.; Tran, H.T. Surface-protective assistance of ultrasound in synthesis of superparamagnetic magnetite nanoparticles and in preparation of mono-core magnetite-silica nanocomposites. *Journal of Science: Advanced Materials and Devices* **2018**, 3, 323-330.
18. Ahamed, M.; Akhtar, M. J.; Alhadlaq, H.A.; Khan, M.A.M.; Alrokayan, S.A. Comparative cytotoxic response of nickel ferrite nanoparticles in human liver HepG2 and breast MFC-7 cancer cells. *Chemosphere* **2015**,135, 278-288.
19. Balakrishnan, P.B.; Silvestri, N.; Fernandez-Cabada, T.; Marinaro, F.; Fernandes, S.; Fiorito, S.; Miscuglio, M.; Serantes, D.; Ruta, S.; Livesey, K.; Hovorka, O.; Chantrell, R.; Pellegrino, T. Exploiting Unique Alignment of Cobalt Ferrite Nanoparticles, Mild Hyperthermia, and Controlled Intrinsic Cobalt Toxicity for Cancer Therapy. *Adv. Mater.* **2020**, 32, 2003712.
20. Yu, Z.; Grasso, M.F.; Cui, X.; Silva, R.N.; Zhang, P. Sensitive and Label-Free SERS Detection of Single-Stranded DNA Assisted by Silver Nanoparticles and Gold-Coated Magnetic Nanoparticles. *ACS Appl. Bio. Mater.* **2020**,3,2626-2632.
21. Lone, S.A.; Sanyal, P.; Das, P.; Sadhu, K.K. Citrate Stabilized Au-FexOy Nanocomposites for Variable Exchange Bias, Catalytic Properties and Reversible Interaction with Doxorubicin. *ChemistrySelect* **2019**, 4, 8237-8245.
22. Félix, L.L.; Sanz, B.; Sebastián, V.; Torres, T.E.; Sousa, M.H.; Coaquira, J.A.H.; Ibarra, M.R.; Goya, G.F. Gold-decorated magnetic nanoparticles design for hyperthermia applications and as a potential platform for their surface-functionalization. *Scientific reports* **2019**, 9, 1-11.
23. Xie, L.; Qian, W.; Yang, S.; Sun, J.; Gong, T. A facile and green synthetic route for preparation of heterostructure Fe3O4@Au nanocomposites. *MATEC Web of Conferences. EDP Sciences* **2017**, 88, 02001.
24. Li, Z.H.; Bai, J.H.; Zhang, X.; Lv, J.M.; Fan, C.S.; Zhao, Y.M.; Wu, Z.L.; Xu, H.J. Facile synthesis of Au nanoparticle-coated Fe3O4 magnetic composite nanospheres and their application in SERS detection of malachite green. *Spectrochimica Acta Part A: Molecular and Biomolecular Spectroscopy* **2020**, 241, 118532.
25. Liua, X.; Yanga, X.; Lic, K.; Liua, H.; Xiaoa, R.; Wanga, W.; Wanga, C.; Wang, S. Fe3O4@Au SERS tags-based lateral flow assay for simultaneous detection of serum amyloid A and C-reactive protein in unprocessed blood sample. *Sensors and Actuators B: Chemical* **2020**, 320, 128350.
26. Chen, Y.; Zhang, Y.; Kou, Q.; Liu, Y.; Han, D.; Wang, D.; Sun, Y.; Zhang, Y.; Wang, Y.; Lu, Z.; Chen, L.; Yang, J.; Xing, S.G. Enhanced catalytic reduction of 4-nitrophenol driven by Fe3O4-Au magnetic nanocomposite interface engineering: From facile preparation to recyclable application. *Nanomaterials* **2018**, 8, 353.

27. Kheradmand, E.; Poursalehi, R.; Delavari, H. Optical and magnetic properties of iron-enriched Fe/FexOy@Au magnetoplasmonic nanostructures. *Applied Nanoscience* **2020**, 10,1083-1094.
28. Huang, W.-C.; Tsai, P.-J.; Chen, Y.-C. Multifunctional Fe3O4@Au nanoeggs as photothermal agents for selective killing of nosocomial and antibiotic-resistant bacteria. *Small* **2009**, 5, 51-56.
29. El-Sayed, H.M. Evidence on the presence of Ruderman–Kittel–Kasuya–Yosida (RKKY) interaction in CoFe2O4@Au nano structure. *Superlattices Microstruct.* **2016**, 91, 98-104.
30. Ghorbani, M.; Mahmoodzadeh, F.; Nezhad-Mokhtari, P.; Hamishehkar, H. A novel polymeric micelle-decorated Fe3O4/Au core–shell nanoparticle for pH and reduction-responsive intracellular co-delivery of doxorubicin and 6-mercaptopurine. *New J. Chem.* **2018**, 42, 18038-18049.
31. Mikalauskaite, A.; Kondrotas, R.; Niaura, G.; Jagminas, A. Gold-coated cobalt ferrite nanoparticles via methionine-induced reduction. *J. Phys. Chem. C* **2015**, 119, 17398-17407.
32. Li, Y.; Liu, J.; Zhong, Y.; Zhang, J.; Wang, Z.; Wang, L.; An, Y.; Lin, M.; Gao, Z.; Zhang, D. Biocompatibility of Fe3O4@Au composite magnetic nanoparticles in vitro and in vivo. Int. *J. Nanomed.* **2011**, 6, 2805-2819.
33. Jagminas, A.; Mažeika, K.; Kondrotas, R.; Kurtinaitienė, M.; Jagminienė, A.; Mikalauskaitė, A. Functionalization of cobalt ferrite nanoparticles by a vitamin C-assisted covering with gold. *Nanomaterials and Nanotechnology*. **2014**, 4, 11.
34. Zeng, J.; Gong, M.; Wang, D.; Li, M.; Xu, W.; Li, Z.; Li, S.; Zhang, D.; Yan, Z.; Yin, Y. Direct Synthesis of Water-Dispersible Magnetic/Plasmonic Heteronanostructures for Multimodality Biomedical Imaging. *Nano lett.* **2019**, 19, 3011-3018.
35. Evsevskaya, N.; Pikurova, E.; Saikova, S.V.; Nemtsev, I.V. Effect of the Deposition Conditions on the Anion Resin Exchange Precipitation of Indium (III) Hydroxide. *ACS Omega* **2020**, 5, 4542-4547.
36. Saikova. S.V.; Kirshneva, E.A.; Panteleeva, M.V.; Pikurova, E.V.; Evsevskaya, N.P. Production of Gadolinium Iron Garnet by Anion Resin Exchange Precipitation. *Russ. J. Inorg. Chem.* **2019**, 64, 1191-1198.
37. Saikova, S.V.; Trofimova, T.V.; Pavlikov, A.Yu.; Samoilo, A.S. Effect of Polysaccharide Additions on the Anion-Exchange Deposition of Cobalt Ferrite Nanoparticles. *Russ. J. Inorg. Chem.* **2020,** 65, 291-298.
38. Saykova, D.; Saikova, S.; Mikhlin, Y.; Panteleeva, M.; Ivantsov, R.; Belova, E. Synthesis and Characterization of Core–Shell Magnetic Nanoparticles NiFe2O4@Au. *Metals* **2020**,10,1075.
39. Balakrishnan, G.; Barnett, G.V.; Kar, S.R.; Das, T.K. Detection and identification of the vibrational markers for the quantification of methionine oxidation in therapeutic proteins. *Anal. Chem.* **2018**, 90, 6959-6966.
40. [Khoury, R.A.; Ranasinghe, J.C.; Dikkumbura, A.S.; Hamal, P.; Kumal, R.R.; Karam, T.E.; Smith, H.T.; Haber, L.H. Monitoring the Seed-Mediated Growth of Gold Nanoparticles Using in Situ Second Harmonic Generation and Extinction Spectroscopy. *J. Phys. Chem*. **2018**, 122, 24400–24406
41. Kim, G.; Weiss, S.J.; Levine, R.L. Methionine oxidation and reduction in proteins. *Biochim. Biophys. Acta* **2014**,1840, 901-905.
42. Angelova, P.; Solel, E.; Parvari, G.; Turchanin, A.; Botoshansky, M.; Gölzhauser, A.; Keinan, E. Chemisorbed monolayers of corannulene penta-thioethers on gold. *Langmui*r **2013**, 29, 2217-2223.
43. Chen, K.; Li, H.; Xu, Y.; Liu, K.; Li, H.; Xu, X.; Qiu, X.; Liu, M. Untying thioether bond structures enabled by "voltage-scissors" for stable room temperature sodium–sulfur batteries. *Nanoscale* **2019**, 11, 5967-5973.
44. Bergès, J.; de Oliveira, P.; Fourré, I.; Houée-Levin, C. The one-electron reduction potential of methionine-containing peptides depends on the sequence. *J. Phys. Chem. B* **2012**, 116, 9352-9362.
45. Stein, C.R.; Bezerra, M.T.S.; Holanda, G.H.A.; André-Filho, J.; Morais, P.C. Structural and magnetic properties of cobalt ferrite nanoparticles synthesized by co-precipitation at increasing temperatures. *AIP Adv.* **2018**, 8, 056303.
46. Ammar, S.; Helfen, A.; Jouini, N.; Fiévet, F.; Rosenman, I.; Villain, F.; Molinie, P.; Danot, M. Magnetic properties of ultrafine cobalt ferrite particles synthesized by hydrolysis in a polyol medium. *J. Mater. Chem.* **2001**, 11,186 -192.
47. Labchir, N.; Hannour, A.; Hssi, A.A.; Vincent, D.; Chatelon, J.P.; Dufeu, D.; Ihlal, A.; Sajieddine, M. Microwave response of coplanar waveguide based on electrodeposited CoFe2O4 nanowires. *Journal of Magnetism and Magnetic Materials* **2020**, 510, 166952.
48. Grigorova, M.; Blythe, H.J.; Blaskov, V.; Rusanov, V.; Petkov, V.; Masheva, V.; Nihtianova, D.; Martinez, Ll.M.;, Muñoze, J.S.; Mikhov, M. Magnetic properties and Mössbauer spectra of nanosized CoFe2O4 powders. *Journal of Magnetism and Magnetic Materials* **1998**, 183, 163-172.
49. Ghobadifard, M.; Farhadi, S.; Mohebbi, S. Sonocatalytic performance of magnetic flower-like CoFe2O4 nanoparticles prepared from a heterometallic oxo-centered trinuclear complex under microwave irradiation. *Polyhedron* **2018**, 155, 66–76.
50. Peddis, D.; Yaacoub, N.; Ferretti, M.; Martinelli, A.; Piccaluga, G.; Musinu, A.; Cannas, C.; Navarra, G.; Greneche, J.M.; Fiorani, D. Cationic distribution and spin canting in CoFe2O4 nanoparticles. *J. Phys.: Condens. Matter.* **2011**, 23, 426004.
51. Wang, Y.-C.; Tang, F.-Y.; Chen, S.-Y.; Chen, Y.-M.; Chiang, E.-P.I. Glycine-N methyltransferase expression in HepG2 cells is involved in methyl group homeostasis by regulating transmethylation kinetics and DNA methylation. *J. Nutr.* **2011**, 141, 777-782.
52. Ligthart-Melis, G.C.; Engelen, M.P.K.J.; Simbo, S.Y.; Have, G.A.M.T.; Thaden, J.J.; Cynober, L.; Deutz ,Ni.E.P. Metabolic consequences of supplemented methionine in a clinical context. *J. Nutr.* **2020**, 150, 2538S-2547S.
53. Elango, R. Methionine nutrition and metabolism: insights from animal studies to inform human nutrition. *J. Nutr.* **2020**, 150, 2518S-2523S.
54. Borges, P.T.; Brissos,V.; Hernandez, G.; Masgrau, L.; Lucas, M.F.; Monza, E.; Frazão, C.; Cordeiro, T.; Martins, L.O. The Methionine-Rich Loop of Multicopper Oxidase McoA follows Open-To-Close Transitions with a Role in Enzyme Catalysis. *ACS Catal.* **2020**, 10, 7162-7176.

55. Biggs, G.S.; Klein, O.J.; Boss, S.R.; Barker, P.D. Unlocking the Full Evolutionary Potential of Artificial Metalloenzymes Through Direct Metal-Protein Coordination. *Johnson Matthey Technol. Rev.* **2020**, 64, 407-418.
56. Glišić, B.Đ.; Djuran, M.I.; Stanić, Z.D.; Rajković, S. Oxidation of methionine residue in Gly-Met dipeptide induced by [Au(en)Cl2]+ and influence ofthe chelated ligand on the rate of this redox process. *Gold Bull.* **2014**, 47, 33-40.
57. Vujačić, A.V.; Savić, J.Z.; Sovilj, S.P.; Mészáros Szécsényi, K.; Todorović, N.; Petković, M.Ž.; Vasić, V.M. Mechanism of complex formation between [AuCl4]− and L-methionine. *Polyhedron* **2009**, 28, 593-599.
58. Natile, G.; Bordignon, E.; Cattalini, L. Chloroauric acid as oxidant Stereospecific oxidation of methionine to methionine sulfoxide. *Inorganic Chemistry* **1976**, 15, 246–248.
59. Scuderi, D.; Bergè, J.; de Oliveira, P.; Houée-Levin, C. Methionine one-electron oxidation: Coherent contributions from radiolysis, IRMPD spectroscopy, DFT calculations and electrochemistry. *Radiation Physics and Chemistry* **2016**, 128, 103-111.
60. Asmus, K.D. Stabilization of oxidized sulfur centers in organic sulfides. Radical cations and odd-electron sulfur-sulfur bonds. *Acc. Chem. Res.* **1979**, 12, 436-442.
61. Asmus, K.D. Heteroatom-centered free radicals some selected contributions by radiation chemistry. *Stud. Phys. Theor. Chem.* **2001**, 87, 341-393.
62. Archirel, P.; Houée-Lévin, C.; Marignier, J.-L. Oxidation of Two Inverse Dipeptides, Methionine–Valine and Valine–Methionine: A Joint Experimental and Computational Study. *J. Phys. Chem. B* **2019**, 123, 9087-9097.
63. Fourré, I.; Berges, J.; Houée-Levin, C. Structural and topological studies of methionine radical cations in dipeptides: electron sharing in two-center three-electron bond. *J. Phys. Chem. A* **2010**, 114, 7359-7368.
64. Lam, E.; Hrapovic, S.; Majid, E.; Chong, J.H.; Luong, J.H.T. Catalysis using gold nanoparticles decorated on nanocrystalline cellulose. *Nanoscale* **2012**, 4, 997.
65. Kannan, A.; Rajakumar, P. Synthesis and catalytic application of glycodendrimers decorated with gold nanoparticles–reduction of 4-nitrophenol. *RSC Adv.* **2015**, 5, 46908-46915.
66. Nghiem, T.H.L.; Le, T.N.; Do, T.H.; Vu, T.T.D.; Do, Q.H.; Tran, H.N. Preparation and characterization of silica–gold core–shell nanoparticles. J. *Nanopart. Res.* **2013**, 15, 2091.
67. Goon, I.Y.; Lai, L.M.H.; Lim, M.; Munroe, P.; Gooding, J.J.; Amal, R. Fabrication and Dispersion of Gold-Shell-Protected Magnetite Nanoparticles: Systematic Control Using Polyethyleneimine. *Chem. Mater.* **2009**, 21, 673–681.
68. Martínez-Banderas, A.I.; Aires, A.; Quintanilla, M.; Holguín-Lerma, J.A.; Lozano-Pedraza, C.; Teran, F.J.; Moreno, J.A.; Perez, J.E.; Ooi, B.S.; Ravasi, T.; Merzaban, J.S.; Cortajarena, A.L.; Kosel, J. Iron-Based Core–Shell Nanowires for Combinatorial Drug Delivery and Photothermal and Magnetic Therapy. *ACS Appl. Mater. Interfaces* **2019**, 11, 43976-43988.